Supporting Information

Towards Fast and Durable Anodes for Sodium-/Potassium-ion Hybrid Capacitors: Tailoring Self-Adaptive Nanocages inside the Hybrid Fibers on High Alignment

Dukang Yan,[a,b,c] Mingxue Xie,[a,b,c] Yiying Shao,[c] Meng Chen[a,b], Sen Zhang,[a,b,*] Chao Deng[c,*]

[a] College of Material Science and Chemical Engineering, Harbin Engineering University, Harbin 150001, Heilongjiang, China

[b] State Key Laboratory of Advanced Chemical Power Sources, Guizhou Meiling Power Sources Co. Ltd., Zunyi, Guizhou 563003, China

[c] Key Laboratory for Photonic and Electronic Bandgap Materials, Ministry of Education, Harbin, 150025, Heilongjiang, China

* E-Mail: senzhang@hrbeu.edu.cn (S. Z.)

* E-Mail: chaodenghsd@126.com (C. D.)

Part I: Experimental details, Calculations & Discussions

S-1-1: Preparation of the Iron-based SAAF hybrid fiber

i) Preparation of the electrospun precursor

The electrospinning precursor was prepared by an electrospinning technique. The dual-nozzle with coaxial structure was used in the electrospinning. The shell solution was prepared by dissolving polyvinyl pyrrolidone (PVP, MW:1300000, Aladdin, Shanghai, China) in ethanol (Aladdin, Shanghai, China). The core solution was prepared by mixing the iron oxide nanocube with the PMMA solution. The iron oxide (Fe_2O_3) nanocubes were prepared by a hydrothermal synthesis.[S1] Poly(methyl methacrylate) (PMMA, Aladdin, Shanghai, China) was dissolving in the N, N-dimethylformamide (DMF) to make a uniform solution. The iron oxide nanocubes were added into the PMMA solution under strong stirring to form the core solution. The dual-nozzle was constructed by two coaxial needles, *i.e.* the 23-gauge inner needle (OD: 0.63 mm, ID: 0.33 mm) and the 17-gauge outer needle (OD: 1.47 mm, ID: 1.07 mm). The core solution was loaded into the syringe connected to the inner channel of the dual nozzle and the shell solution was loaded into the syringe connected to the outer channel. The resulting precursor was transferred into a syringe connected to a stainless steel needle. The high potential was applied on the needle relative to a high-rate rotating drum collector. After the electrospinning process, the film was peeled off from the collector and the precursor was obtained.

ii) Preparation of the intermediate product

The prepared electrospun precursor was firstly stabilized at 250 ^{o}C in air. Then the resultant product was calcinated at 700 ^{o}C in N_2 atmosphere with a heating rate of 2 ^{o}C min^{-1}. The resultant product was etched in a diluted hydrochloric acid solution with controlled time at room temperature under magnetic stirring. Then it was washed by distilled water until the filtrate is neutral. After dried at 60 ^{o}C in an oven, the intermediate product is prepared.

iii) Preparation of the FeSe$_2$ based SAAF hybrid fiber

All the iron-based SAAF hybrid fiber was prepared by the vapor phase conversion process. For the preparation of the FeSe$_2$ based SAAF hybrid fiber, the intermediate product and excess amount of Se powders were put into the covered quartz boat and sealed into a tube furnace. It was firstly annealed at 350 ^{o}C for 2 hours, and then elevated to 500 ^{o}C in the H$_2$/Ar atmosphere.

iv) Preparation of FeS$_2$ SAAF hybrid fiber

For the preparation of the FeS$_2$ based SAAF hybrid fiber, sulfur powder was dissolved into carbon bisulfide to get a solution. Then, the solution was dropped on the intermediate product. After the solvent was evaporated, the film was put in a covered quartz boat and sealed in a tube furnance. It was initially kept at 155 ^{o}C for 10 hours, and then elevated to 400 ^{o}C for another 4 hours in Ar atmosphere to produce the final product.

v) Preparation of the FeP SAAF hybrid fiber

For the preparation of the FeP based SAAF hybrid fiber, NaH$_2$PO$_2$ and the intermediate product were put in a covered quartz boats and sealed in a tube furnace. It was firstly

annealed at 300 °C for 2 hours, and then elevated to 600 °C in Ar atmosphere to produce the final product.

vi) Preparation of the FeO_x SAAF hybrid fiber

For the preparation of the FeO_x based SAAF hybrid fiber, the intermediate product were annealed at 260 °C in air.

S-1-2: Preparation of the RF and CC reference samples

i) Preparation of the RF reference sample

The RF reference sample was prepared by the same selenization process (S-1-1-*iii*) as the $FeSe_2$ SAAF fiber with the Fe_2O_3 nanocube as the precursor.

ii) Preparation of the CC reference sample

Firstly, the carbon coated iron oxide nanocube is prepared. The Fe_2O_3 nanocube was dispersed in the mixed solution of water and ethyl alcohol. After continuous ultrasonic stirring in water bath for ten minutes, ammonia was added into the mixture under stirring. Then resorcinol was dissolved in the above solution for another ten minutes, followed by adding formalin and stirring for five hours. After washed with water and ethanol several times, the resultant product was collected. Then, the obtained powder was annealed at 550 °C for 4 hours in Ar/H_2 atmosphere. Secondly, the prepared carbon coated iron oxide was used as the precursor to selenization in the same way as the SAAF fiber (S-1-1-*iii*) to make the CC reference sample.

S-1-3: Preparation of the hierarchical carbon fiber (HCF) cathode

In the S-1-2, the cores in the nanocubes inside the fibers of the intermediate product are fully removed by prolonging the etching time to two days. Then the resultant film was

washed with distilled water, followed by dring in the oven overnight. Finally, the pure carbon host was achieved.

S-2: Materials characterizations

Powder X-ray diffraction (XRD, Bruker D8/Germany) using Cu Kα radiation was employed to identify the crystalline phase of the material. The morphology was observed with a scanning electron microscope (SEM, HITACHIS-4700) and a transmission electron microscope (TEM, JEOS-2010 PHILIPS). The element distribution of the sample was confirmed by energy dispersive X-ray detector (EDX). X-ray photoelectron spectroscopy (XPS, Thermo ESCALAB 250) was employed to measure the chemical or electronic state of each element. Thermogravimetric analysis (TGA, NETZSCH STA 449C) was used to investigate the carbon content of the sample. Nitrogen adsorption-desorption isotherms were measured using a Micromeritics ASAP 2010. Specific surface area was calculated using the Brunauer-Emmett-Teller (BET) method.

S-3: Electrochemical measurements

S-3-1: Electrochemical properties in sodium/potassium half cell

The electrochemical characteristics in sodium ion battery were measured in CR2032 coin cells. The coin cells were assembled in an argon filled glove box. The SAAF hybrid fiber was directly used as electrode and the sodium/potassium film worked as the counter electrode. Glass fiber was used as the separator. The electrolytes of potassium bis(fluorosulfonyl)imide (KFSI) and $NaClO_4$ were used in the potassium-ion and sodium-ion systems. The galvanostatic charge/discharge cycling was tested by a Land battery testing system (Wuhan, China). CV and EIS measurements were conducted using a Zivelab electrochemical workstation.

S-3-2: Electrochemical properties in SIHC and PIHC

The SIHC and PIHC were fabricated with the SAAF fiber as anode and the HCF fiber as cathode. Glass fiber was used as the separator. Potassium bis(fluorosulfonyl)imide (KFSI) and $NaClO_4$ were used as electrolytes for PIHC and SIHC. Before the assembling of the full device, the anode was activated in a half cell by five charge/discharge cycles. The cathode/separator/anode sandwich was put into an aluminum plastic bag to assemble the sandwich-type cell. After the electrolytes were injected, the cells were vacuum sealed.

S-4: Calculation of the capacitive contribution

In the CV curves, the current is believed to originate from two independent and distinct parts: the surface-induced capacitive process and the diffusion-controlled process. As described in the following equation,[S2,S3]

$$i = a \times v^b \tag{1}$$

Where i is the measured current; v is the scan rate. Determined from the slope of the curve between the $\log i$ versus $\log v$, the b values of different peaks can be achieved.

$$\log i = \log a + b \log v \tag{2}$$

The b values vary from 0.5 to 1. When b value is 0.5, it indicates a diffusion-controlled process; when b value is 1.0, it suggests a complete capacitive process. To further characterize each contribution to the total properties, the measured current (i) at a fixed potential can be separated into two parts, $i.\ e.$ the contribution from the capacitive and the diffusion processes as described in the following equation,

$$i = k_1 v + k_2 v^{1/2} \tag{3}$$

Where $k_1 v$ and $k_2 v^{1/2}$ correspond to the capacitive and diffusion contributions,

respectively. Based on the above equation, the ratios of the capacitive contribution ratios at various scan rates can be quantitatively achieved.

S-5 Computational methods

The theoretical calculations were carried out using the density functional theory and the plane-wave pseudpotential method [S4]. The generalized gradient approximation (GGA) of the Perdew-Burke-Ernzerhof (PBE) exchange correlation function [S5] was adopted. All geometric optimizations and energy calculations were performed using periodic boundary conditions with adjacent adsorbents and adsorbents to prevent configurational interactions.

Part II: Supporting Figures

Figure S1
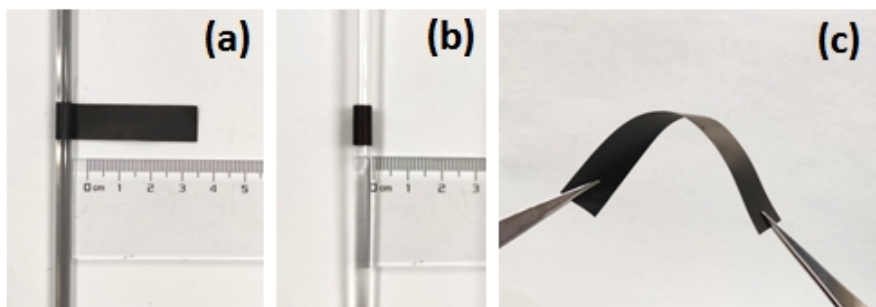
Figure S1 Digital images of the flexible SAAF hybrid fiber in low (a) and high (b)

degrees of curving states and bended (c) states.

Figure S2
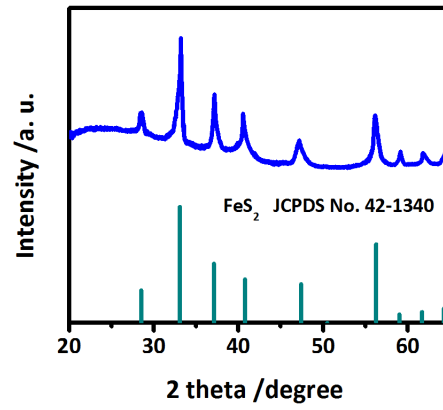
Figure S2 XRD pattern of the FeS_2@C based SAAF hybrid fibers. The standard pattern of FeS_2 is shown as insert.

Figure S3
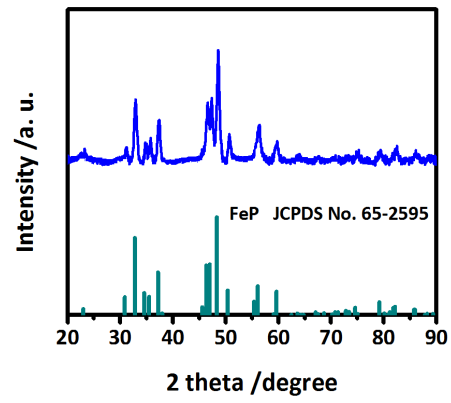
Figure S3 XRD pattern of the FeP@C based SAAF hybrid fibers. The standard pattern of
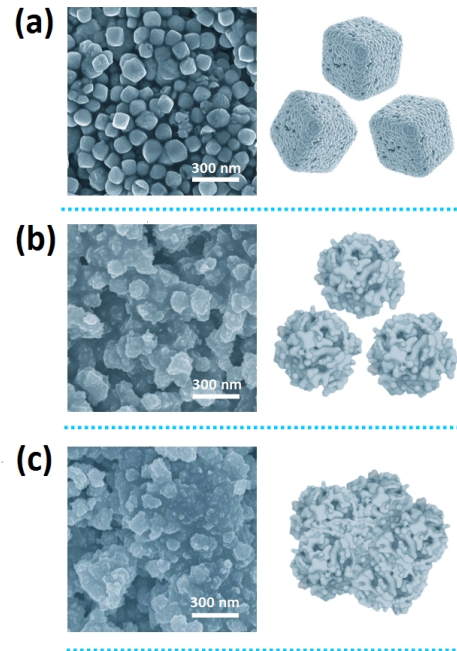
FeP is shown as insert.

Figure S4
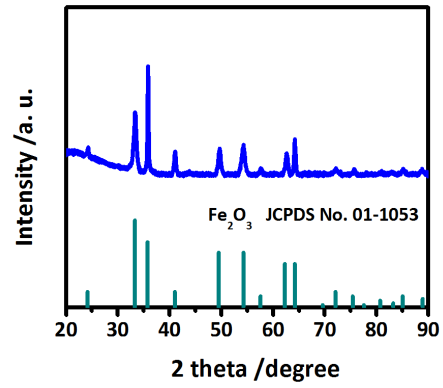
Figure S4 XRD pattern of the FeO$_x$@C based SAAF hybrid fibers. The standard pattern

of Fe$_2$O$_3$ is shown as insert.

Figure S5

Figure S5 SEM images (left) and schematic illustrations (right) of the RF reference sample in pristine state (a), after five cycles (b) and after twenty cycles (c).

Figure S6
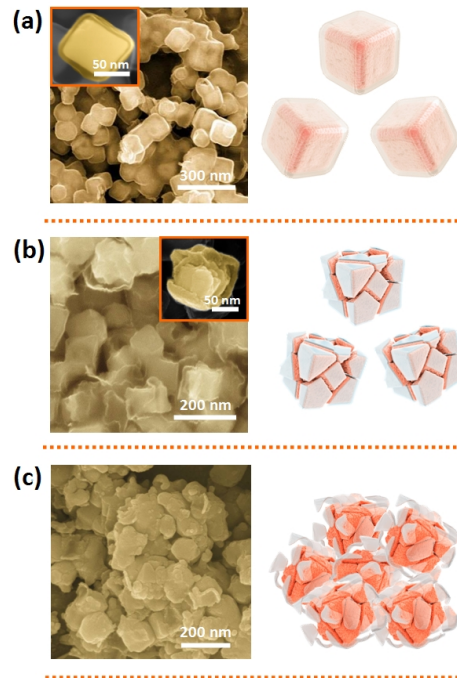
Figure S6 SEM images (left) and schematic illustrations (right) of the CC reference sample in pristine state (a), after fifty cycles (b) and after one hundred cycles (c).

Figure S7
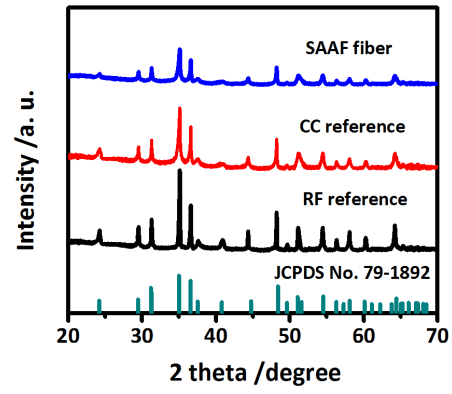
Figure S7 XRD patterns of the CC and RF reference samples in comparison to the FeSe$_2$ SAAF hybrid fibers. The standard pattern of FeSe$_2$ is shown as insert.

Figure S8
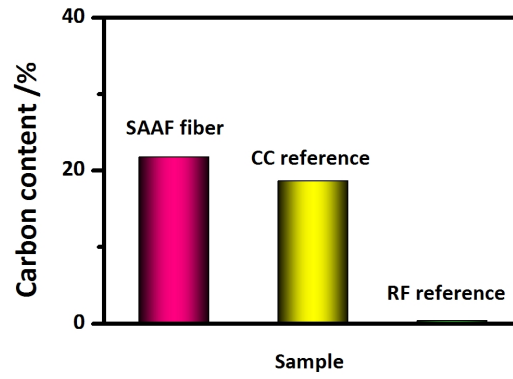
Figure S8 Comparison of the carbon contents for the FeSe$_2$ SAAF hybrid fiber, CC reference and RF reference samples.

Figure S9
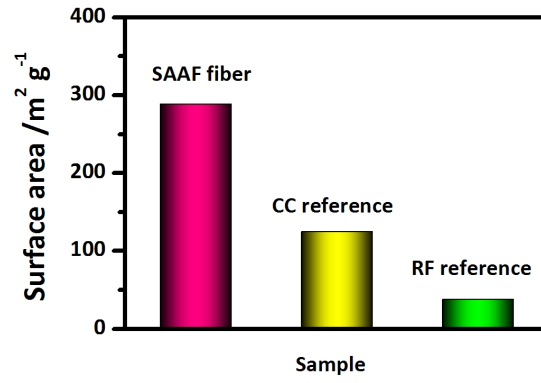
Figure S9 Comparison of the surface areas for the FeSe$_2$ SAAF hybrid fiber, CC reference and RF reference samples.
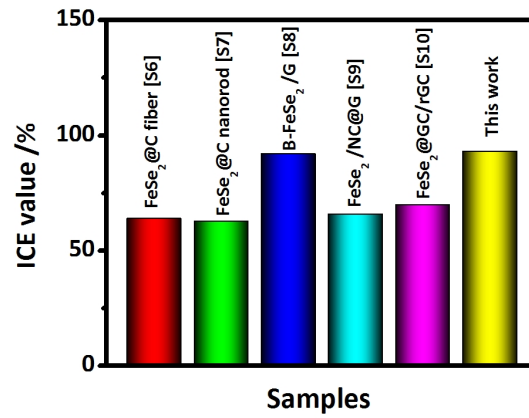
Figure S10

Figure S10 Comparison of the ICE values between the SAAF hybrid fiber in the present work and the $FeSe_2$ based materials in previous reports[S6~S10].
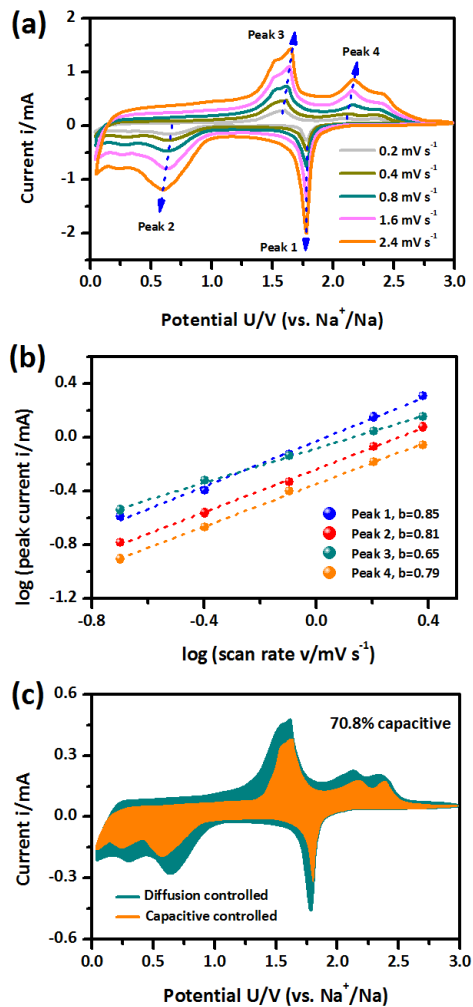
Figure S11 (a) CV curves of the FeSe$_2$ SAAF fibers at a series of scan rates from 0.2 to 2.4 mV s^{-1}; (b) relationship between the logarithm peak current and logarithm scan rates; (c) capacitive and diffusion contributions in the CV curves at 0.4 mV s^{-1}
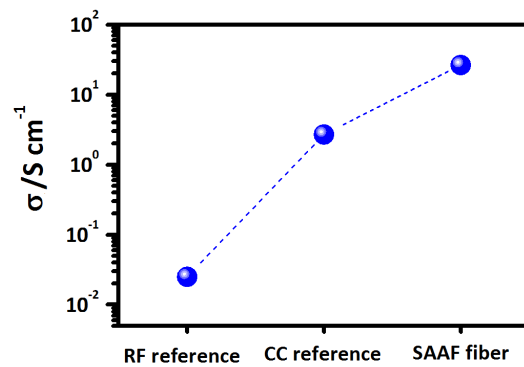
Figure S12

Figure S12 Comparison of the electronic conductivities of the $FeSe_2$ SAAF hybrid fiber, CC reference and RF reference samples.
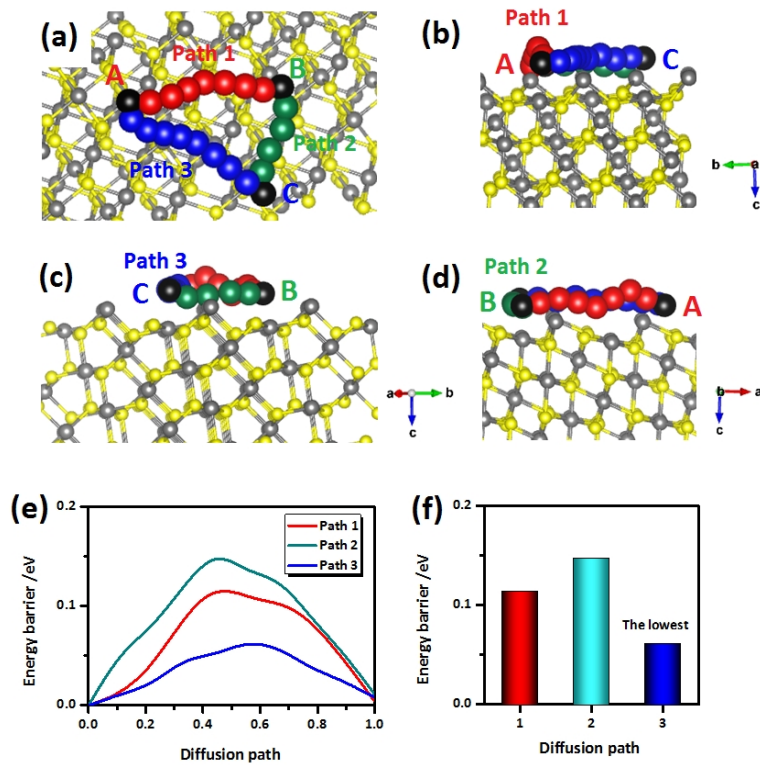
Figure S13

Figure S13 (a) Top view and (b~d) side views on schematic representation of corresponding diffusion pathways (path 1, 2 and 3) for potassium ion on FeSe$_2$ (111) surface. (e) Energy profiles for three different diffusion processes and (f) the corresponding energy barriers of a potassium ion on the FeSe$_2$ (111) surface.
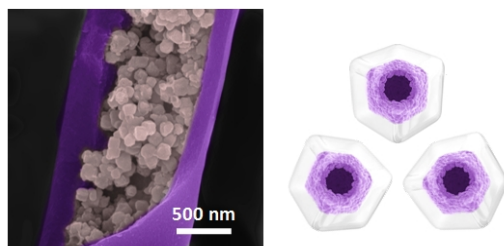
Figure S14

Figure S14 SEM image (left) and schematic illustration (right) of the SAAF sample after

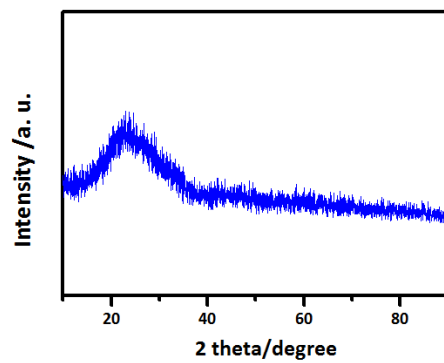three hundred cycles.

Figure S15

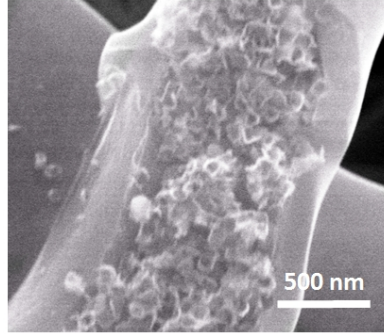Figure S15 XRD pattern of the hierarchical carbon based fiber.

Figure S16

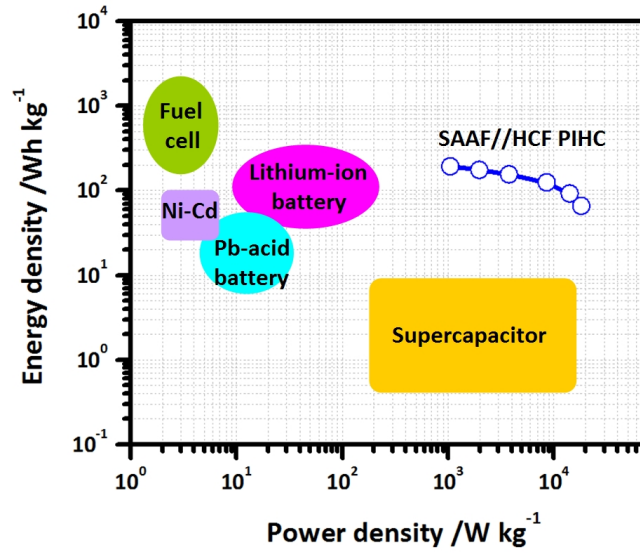Figure S16 SEM image of the hierarchical carbon based fiber.

Figure S17

Figure S17 Ragone plot of the SAAF//HCF PIHC in comparison with commercial energy storage devices.[S11]

Part III: Supporting References

[S1] R. M. Liu, Y. W. Jiang, H. Fan, Q. Y. Lu, W. Du, F. Gao, *Chem. Eur. J* **2012**, *18*, 8957-8963.

[S2] J. G. Wang, H. Y. Liu, R. Zhou, X. R. Liu, B. Q. Wei, *J. Power Sources* **2019**, *413*, 327-333.

[S3] H. H. Sun, J. G. Wang, Y. Zhang, W. Hua, Y. Y. Li, H. Y. Liu, *J. Mater. Chem. A* **2018**, *6*, 13419-13427.

[S4] J. Wang, J. Polleux, J. Lim, B. Dunn, *J. Phys. Chem. C* **2007**, *111*, 14925-14931.

[S5] B. K. Lesel, J. S. Ko, B. Dunn, S. H. Tolbert, *ACS Nano* **2016**, *10*, 7572-7581.

[S6] T. X. Wang, W. T. Guo, G. Wang, H. Wang, J. T. Bai, B. B. Wang, *J. Alloys Compd.* **2020**, *834*, 155265.

[S7] H. S. Fan, H. Yu, Y. F. Zhang, J. Guo, Z. Wang, H. Wang, N. Zhao, Y. Zheng, C. F. Du, Z. F. Dai, Q. Y. Yan, J. Xu, *Energy Storage Mater.* **2018**, *10*, 48-55.

[S8] G. S. An, Y. F. Yuan, B. Zhang, L. B. Tang, B. Xiao, Z. J. He, J. C. Zheng, J. Lu, *Adv. Energy Mater.* **2019**, *9*, 1900356.

[S9] S. K. Jiang, M. J. Xiang, J. Y. Zhang, S. Q. Chu, A. Marcelli, W. S. Chu, D. J. Wu, B. Qian, S. Tao, L. Song, *Nanoscale* **2020**, *12*, 22210.

[S10] J. S. Cho, J. K. Lee, Y. C. Kang, *Sci. Rep.* **2016**, *6*, 23699.

[S11] X. Hu, G. B. Zhong, J. W. Li, Y. J. Liu, J. Yuan, J. X. Chen, H. B. Zhan, Z. H. Wei, *Energy Environ. Sci.* **2020**, *13*, 2431-2440.